Available online at www.sciencedirect.com
SCIENCE DIRECT®
Catena 52 (2003) 273–288
CATENA
www.elsevier.com/locate/catena

Spatial modeling of wind speed around windbreaks

Olga Vigiak[a,*], Geert Sterk[a], Andrew Warren[b], Lawrence J. Hagen[c]

[a] *Erosion and Soil and Water Conservation Group, Department of Environmental Sciences, Wageningen University, Nieuwe Kanaal 11, 6709 PA Wageningen, The Netherlands*
[b] *Department of Geography, University College London, 26 Bedford Way, London WC1H 0AP, UK*
[c] *USDA-ARS Wind Erosion Research Unit, Throckmorton Hall, Kansas State University, Manhattan, KS 66506, USA*

Abstract

This paper presents a model to integrate windbreak shelter effects into a Geographic Information System (GIS). The GIS procedure incorporates the 1999 version windbreak sub-model of the Wind Erosion Prediction System (WEPS). Windbreak shelter is modeled in terms of friction velocity reduction, which is a function of wind speed and direction, distance from the barrier, windbreak height, porosity, width, and orientation. A first application of the model was conducted at a study area with an extensive windbreak network in England (Thetford, East Anglia). Windbreak characteristics (windbreak type, height, width, porosity, and location) were recorded. Porosity was estimated from digitized B/W silhouettes. To evaluate the network effectiveness, a windbreak network shelter index (SI) was proposed in terms of average reduction of friction velocity over the area due to network shelter. The network was found to give good protection, but the windbreak distribution was not optimal in relation to the wind vector distribution.

Keywords: Windbreak; Wind Erosion Prediction System; GIS; Wind speed reduction; Wind erosion

1. Introduction

Windbreaks have been used for centuries to shelter crops from wind damage and to protect soils from wind erosion. They reduce wind speed and alter the characteristics of airflow around them, inducing changes in the surrounding atmospheric, plant, and soil environments (Cleugh, 1998). The interaction between the windbreak and the airflow is complicated by the turbulent characteristics of the wind and by the complex behavior of

* Corresponding author. Tel.: +31-317-482754; fax: +31-317-484759.
E-mail address: Olga.Vigiak@wur.nl (O. Vigiak).

0341-8162/03/$ - see front matter © 2003 Elsevier Science B.V. All rights reserved.
doi:10.1016/S0341-8162(03)00018-3

natural obstacles. Furthermore, the types of protection given by windbreaks are manifold, being both direct and indirect. Direct effects are due to adsorption of momentum from the wind flow, thus decreasing wind erosivity. They result in reductions of wind speed and turbulence intensity within a certain distance in the lee. Indirect effects consist of microclimatic changes due to alterations of the latent and sensible heat fluxes. Hence, crop development and soil conditions, and thus soil erodibility, are also modified. Indirect effects must be considered within the soil–water–crop system and will not be further discussed here.

The classic wind speed profile across a barrier is shown in Fig. 1. It shows the effects of the two main characteristics of the windbreaks, namely, height and porosity, on wind speed (Heisler and Dewalle, 1988). The area sheltered by the barrier is proportional to windbreak height (h), and horizontal distances are usually expressed in terms of height units (xh). Barrier influence extends from approximately $-5h$ (windward) to $30h$–$35h$ (leeward). The reduction of wind speed is normalized to the speed of the approach flow ($U_{approach}$). The minimum wind speed is achieved in the near lee, at distances around $4h$–$6h$. Further leeward, at around $20h$, wind speed recovers to 80% of the approach wind speed.

The aerodynamic porosity of the windbreak determines the ratio between airflow that passes through the barrier pores (“through-flow”) and airflow that diverges over the barrier (“diverged-flow”). Porosity therefore determines the position of minimum wind speed and the rate of recovery of wind speed. The less porous the barrier, the more effective the protection (Fig. 1). However, very dense barriers (porosity less than 20%) can induce an area of recirculating eddies in the immediate lee, with increased turbulence. For

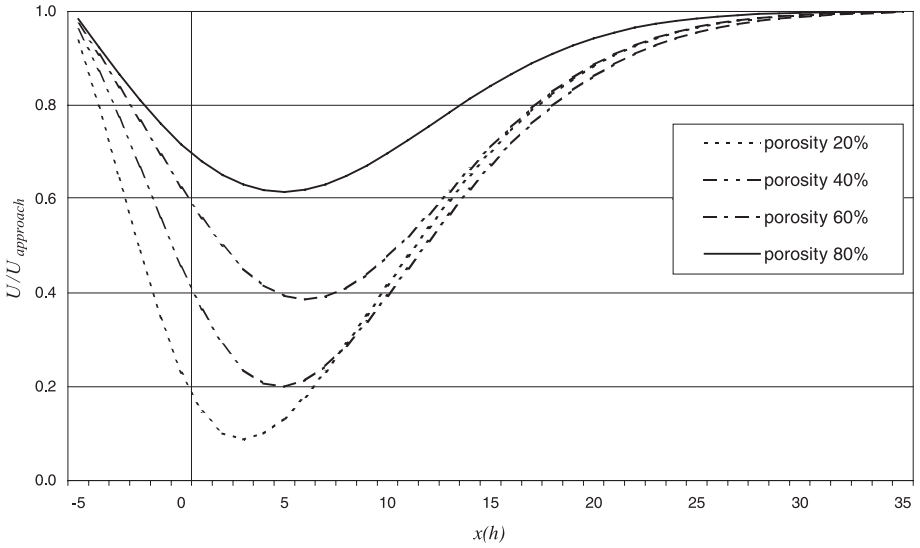

Fig. 1. Wind speed profile across a barrier. The wind speed at any distance (U) is normalized by the approach wind speed ($U_{approach}$) as a function of the horizontal distance from the barrier x in terms of windbreak height units (h) and porosity (from the WEPS barrier subroutine, 1999 version).

such windbreaks, the wind profile shows a lower minimum wind speed. The rate of wind speed recovery is faster in the near lee (between $0h$ and $10h$), and slower afterwards, hence low porosity windbreaks are slightly less effective than medium porosity windbreaks (Wang and Takle, 1997).

It is impractical, at least throughout the landscape, to physically measure the aerodynamic porosity of natural tree windbreaks. Porosity is therefore usually approximated by the measured optical porosity (Loeffler et al., 1992). Generally, aerodynamic porosity and optical porosity are not equivalent, since the latter does not account for the three-dimensional nature of pores through which the wind flows. This is particularly true for broad-leaved windbreaks. However, for thin narrow artificial barriers, optical porosity approximates actual porosity (Heisler and Dewalle, 1988). Loeffler et al. (1992) concluded that optical porosity can be used for field evaluation of the windbreak shelter effect, but they also emphasized that the accuracy of the relationship is highly species-specific.

Besides windbreak height and porosity, the actual form of the wind speed curve depends on other important characteristics of the airflow–windbreak system. These are the approach flow characteristics, such as wind speed, wind direction, turbulence intensity, and atmospheric stability, and external windbreak properties, such as windbreak shape, width, and length (Heisler and Dewalle, 1988). The effects of these factors are important but often contradictory, and they are seldom defined analytically (Cleugh, 1998; McNaughton, 1988; Heisler and Dewalle, 1988).

Local and regional effects of a windbreak network can be distinguished. On a local scale of a few adjacent fields, the second and successive downwind barriers are less effective in wind speed reduction than the first. On a regional scale, windbreak systems increase terrain roughness, which means that a dense network slows down the average wind speed of the region as a whole. This is reflected by an increment in the landscape roughness height value z_0 (Seguin, 1973).

Airflow–windbreak interactions have been described and studied in great detail in some numerical simulation models (Wilson, 1985; Wang and Takle, 1995). These models give insights into airflow around porous barriers. Because of their purpose and the nature of their input data, these models are beyond the scope of this study. On the other hand, windbreaks are seldom treated explicitly in wind erosion models. Exceptions are the Revised Wind Erosion Equation (RWEQ, Fryear et al., 1998) and the Wind Erosion Prediction System (WEPS, Hagen, 1991). In the Revised Wind Erosion Equation (RWEQ), the windbreak effect was recently introduced as percentage of wind speed reduction in the windbreak lee as function of barrier height and optical density. In the Wind Erosion Prediction System (WEPS), windbreak effects are incorporated by a reduction factor of friction velocity that takes into account the distance from the barrier, porosity, and width of the barrier.

To simulate the spatial pattern of wind speed reductions by windbreaks, the windbreak model needs to be linked to a Geographic Information System (GIS). This allows the handling of the variability of the inputs and expresses windbreak effects as a function of the spatial relationship between barrier characteristics, wind direction, and sheltered areas. The main objective of this study was to integrate the WEPS windbreak subroutine into a GIS to simulate wind speed reductions by windbreaks in areas exposed to wind erosion.

2. Materials and methods

2.1. Windbreak model

WEPS is a process-based, daily time-step wind erosion model. It computes soil flux, deposition, and loss from a specific region, consisting of a few fields, over time (Hagen, 1991). The core of the model is the erosion module, which simulates soil loss or deposition due to creep, saltation, and suspension transport. The driving variable for transport is the wind friction velocity u_* (m s^{-1}), which is related to average wind speed $U(z)$ (m s^{-1}) at height z (m) by the logarithmic law (Panofsky and Dutton, 1984):

$$U(z) = \frac{u_*}{k} \ln\left(\frac{z}{z_0}\right) \tag{1}$$

where k is the von Kármán constant (0.4) and z_0 is the roughness height (m). In the WEPS model, friction velocity is calculated in two steps (Hagen, 1995). First, the friction velocity at the weather station (u_*^{WS}) is computed by applying the logarithmic law (Eq. (1)), then the friction velocity at the subregion (field) level u_*^R is calculated with Lettau's equation (Panofsky and Dutton, 1984):

$$u_*^R = u_*^{WS} \left(\frac{z_0^R}{z_0^{WS}}\right)^{0.067} \tag{2}$$

where z_0^R is the roughness height of the subregion and z_0^{WS} is the roughness height at the weather station (assumed to be 25 mm, Hagen, 1995).

The resulting u_*^R is corrected for windbreak effects by means of a windbreak subroutine. The windbreak subroutine calculates a friction velocity reduction factor f_{xh} at any distance in the surrounding area (from $-5h$ windward and up to $35h$ leeward). In the 1999 WEPS version, the reduction factor is defined as:

$$f_{xh} = 1 - \exp[-axh^2] + b\exp[-0.003(xh + c)^d] \tag{3}$$

where xh is the distance from the barrier along the wind direction in barrier heights. Coefficients a, b, c, and d depend on barrier porosity (θ):

$$a = 0.008 - 0.17\theta + 0.17\theta^{1.05} \tag{4}$$

$$b = 1.35\exp(-0.5\theta^{0.2}) \tag{5}$$

$$c = 10(1 - 0.5\theta) \tag{6}$$

$$d = 3 - \theta \tag{7}$$

Barrier porosity is calculated from windbreak optical porosity (op), width (w, average width measured perpendicularly to the main axis of the barrier), and height (h):

$$\theta = \mathrm{op} + 0.02\frac{w}{h} \tag{8}$$

When two barriers influence the same area, the lowest windbreak reduction factor is selected. At any point, the calculated u_*^{R} is multiplied by the reduction factor f_{xh} to obtain the final friction velocity u_*^{F}:

$$u_*^{\mathrm{F}} = f_{xh} u_*^{\mathrm{R}} \tag{9}$$

Whenever the final friction velocity u_*^{F} is above the static threshold friction velocity ($u_{*\mathrm{t}}$) of the soil at the subregion, sediment transport may occur.

2.2. Study area

The study area is a 5 × 5 km experimental site located near Barnham (Thetford, East Anglia, UK), and can be considered representative of the Suffolk/Norfolk landscape in East England (Fig. 2). The area is characterized by sandy soils derived from glacio-fluvial deposits. Arable fields are interspersed with blocks of coniferous woodland. The main crops are winter cereals (wheat and barley), sugar beets, carrots, and potatoes. The worst erosion events occur in fields with carrots and other root crops (Riksen and De Graaff, 2001). Until last century, most of the area was used for extensive grazing. Conversion to arable farming brought with it the need to protect crops from wind damage. Windbreaks have been used for this purpose since that time. Some of them are very wide, which fits them to their secondary purpose of wildlife reserves. At the moment, many of them are poorly maintained and some should be replaced. It is therefore useful to evaluate their current effectiveness.

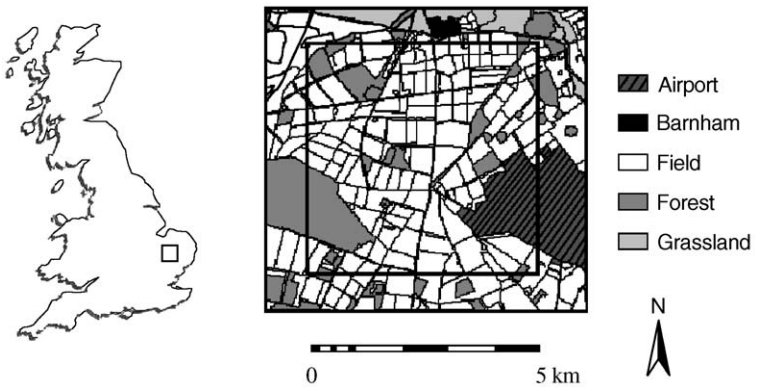

Fig. 2. Study area location and land use (based on Ordnance Survey Mapping with the permission of the controller of HMSO. © Crown. Copyright ED 2813360001).

2.3. Windbreak survey

A windbreak survey was conducted in summer 1999 to define and classify the windbreak network. Six major windbreak types were identified using Drachenfels (1994) classification, which was slightly modified to meet the characteristics of the windbreaks in the area. The following classes were distinguished: hedgerow, hedge, line of coniferous trees, single line of deciduous trees, multiple line of deciduous or mixed trees, and small wood. For each windbreak, the following characteristics were recorded: class, height, width, species composition, and presence of gaps in the crown. Windbreaks were photographed to estimate their optical porosity. Pictures were taken perpendicular to the barrier, keeping the sun behind or far on the side to limit unwanted leaf reflection (Kenney, 1987). An ordinary SLR camera with a 50-mm lens and AGFAPAN APX 100 B/W film was used. Windbreak locations were recorded on aerial photographs of the area (approximate scale 1:1800) and successively transferred on a topographic map (Ordnance Survey 1:50 000 Landranger).

2.4. Porosity estimation

Optical porosity was estimated as average optical porosity for each windbreak class. Two main reasons underlie the choice of using class averages to represent porosity. The first was a practical consideration: the large number of windbreaks in the area would have made the task of estimating single barrier porosity too time-consuming. Second, porosity variability within a natural windbreak is high and, provided that the windbreak types are correctly defined, the error in the class estimation is probably comparable to the error in the individual estimation.

Optical porosity was estimated using Kenney's (1987) digitizing technique. In this procedure, optical porosity is expressed as the ratio of white (empty spaces) to total pixels on the digitized black and white pictures. The technique is capable of estimating optical porosity with a 2% accuracy (Kenney, 1987).

Porosity was calculated as full porosity from the ground to the top of the tallest crown. After scanning the films, the images were stored in digital format. With a photo-elaboration software, sections of the picture above and below the barrier were removed and contrast, brightness, and edge definition were enhanced. Pixel DN (Digital Number, 0–255) frequencies were tabulated and graphically analyzed with an image processing software. DN histograms showed a sharp bimodal distribution. A threshold DN value was introduced to separate windbreak silhouette (interpreted as "black" pixels, DN smaller than the threshold) from background ("white" pixels, DN larger than the threshold). The threshold value was set picture by picture, after a brief investigation on gray tones. Porosity was finally calculated as the ratio of "white" to total pixels.

Sample size was 10 images for each windbreak class, but was enlarged in the case of high in-class variances to reduce the statistical error. Samples included preferential pictures with little background interference and high contrast. This implies that the samples were not extracted at random, but the inclusion of poor images would have reduced the overall accuracy.

Table 1
Roughness height values for land use types of the area

Land use	z_0 (mm)
Bare soil[a]	1
Sugar beet[a]	30
Cereal residues[a]	70
Grass[b]	150
Non-agricultural areas[c]	10 000

[a] Source: direct measurements of wind logarithmic profiles.
[b] Source: Nickling, 1994.
[c] The value of 10 m was assumed to be excluded from the analysis of non-agricultural areas like forest and buildings.

2.5. GIS environment

The barrier network was acquired as line elements (arc cover) in the ArcInfo Geographic Information System (ESRI, 1999). Windbreak length and orientation were estimated for homogenous segments of windbreak with the GIS tool. A land use map layer was already available (Fig. 2). A table of aerodynamic roughness height values for the different land use types, derived from literature data and on site measurements, was linked to the map (Table 1). User-set parameters for the GIS simulation consisted of wind speed $U(z)$, wind direction, and the static threshold friction velocity u_{*t}. The pixel size of raster layers was set to 3 m.

Fig. 3 shows a schematic representation of the GIS model. First, friction velocity for each field was calculated by applying Eqs. (1) and (2). Then the shelter effect of each barrier was simulated. First, the angle of incidence of the wind vector was calculated, then the distance of protection was calculated along the wind vector, by multiplying the distance of protection in Eq. (3) by the cosine of the angle of incidence. When the angle of incidence was less than 5°, i.e. when the barrier was parallel to the wind vector, the windbreak was excluded from the computation. Eq. (3) was calculated for each barrier according to the windbreak height,

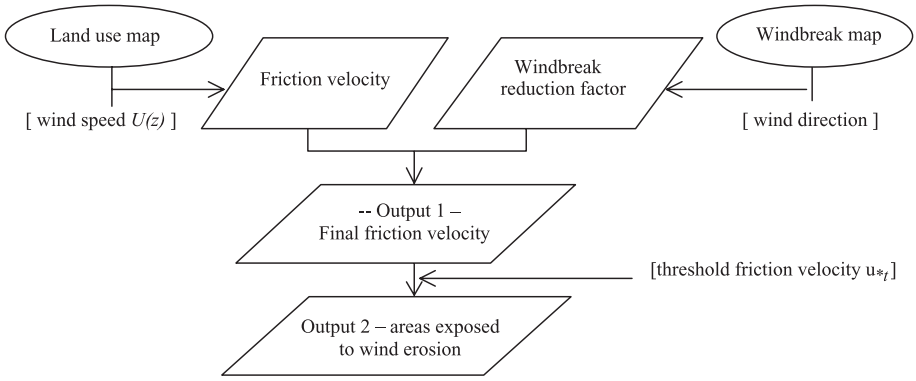

Fig. 3. Schematic representation of the GIS model. The windbreak reduction factor depends on windbreak characteristics and wind direction, but does not depend on wind speed. Terms between rectangular brackets are user-set inputs.

width, and class of porosity (Eqs. (4)–(8)). The procedure was repeated for all the windbreaks present in the area. For areas sheltered by more than one barrier, the minimum reduction factor was selected. Finally, for each point (a grid cell of the raster layer), the field friction velocity was multiplied by the reduction factor to obtain the final friction velocity (Eq. (9)). The main model outputs were two maps. The first map showed the final friction velocity; from this map, friction velocity statistics, i.e. minimum, average, and maximum, could be derived. The second map showed areas exposed to wind erosion risk, i.e. where friction velocity was above the user-defined threshold value u_{*t}.

2.6. Wind speed vectors and network shelter index

To evaluate the windbreak network effectiveness, a comparison between wind speed distribution of the area and windbreak protection was carried out. Data were derived from Honington Station wind records, a 12-year UK Meteorological Office (UKMO) Land Surface Stations database, provided by the British Atmospheric Data Centre (BADC, 2000). Honington Station is located within the study area.

The wind vector r_j in direction j was defined as:

$$r_j = \overline{u}_j d_j \tag{10}$$

where $\bar{u}_j$ is the hourly mean wind speed in direction j (in polar degrees, 0–360°) and d_j is a duration factor, i.e. the average ratio of the number of hours during which wind blows in direction j over the total hours of wind per year. All winds with hourly mean wind speed ū equal or larger than 0.515 m s^{-1} (1 knot) were included in the analysis.

A shelter index was proposed to evaluate the effectiveness of the windbreak network in reducing wind speed for any direction. The shelter index SI_j for direction j was defined as:

$$SI_j = 1 - \frac{\overline{u}^{w}_{*_j}}{\overline{u}_{*_j}} = 1 - \frac{\frac{1}{n}\sum_{i=1}^{n} u^{w}_{*_{ij}}}{\frac{1}{n}\sum_{i=1}^{n} u_{*_{ij}}} \tag{11}$$

where $\bar{u}^{w}_{*j}$ is the mean friction velocity in direction j of the area when windbreaks are present, $\bar{u}_{*j}$ is the mean friction velocity in direction j of the same area assuming the absence of windbreaks, n is the total number of pixels i in the area, u^{w}_{*ij} is the friction velocity of pixel i in direction j when windbreaks are present, and u_{*ij} is the friction velocity of pixel i in direction j in the case of no windbreaks. SI_j gives a value between 0 and 1; it expresses the average reduction in friction velocity over the area due to windbreak protection. The higher the index, the larger the protection offered by the windbreak network along direction j.

For all the j directions that compose the wind rose, a synthetic shelter index SI was computed as a weighted mean shelter index whose weight was proportional to wind speed vector distribution:

$$SI = \sum_j w_j SI_j \tag{12}$$

The weight factor w_j was calculated as:

$$w_j = \frac{r_j}{\sum_j r_j} \tag{13}$$

where r_j is the wind vector in direction j as defined in Eq. (10). In this way, the synthetic shelter index (SI) depends on both the degree of protection given by the windbreaks in any direction and the orientation of the windbreak network in relation to the wind rose in the area.

Wind vectors and shelter indices were computed for 36 wind directions j, each 10°. The simulation parameters were set as follows: wind speed $U(z)$ of 10 m s^{-1} at height z of 10 m, and bare soil condition for all the area (field roughness height z_0^R equal to 0.001 m, Table 1).

3. Results and discussion

3.1. Windbreak network

The windbreak network in the study area is heterogeneous, but well developed. Windbreaks have many purposes, from noise barriers along roads to wildlife reserves. Most of them are quite old, wide, and poorly maintained. The survey led to a classification of six windbreak types that could be considered homogeneous for structure, shape, and species composition. Table 2 shows the total length and the average dimensions of each class. The classes were defined as follows:

(1) Hedgerows (He): mostly low (<3 m). The dominant species is hawthorn (*Crataegus monogyna* L.). Besides ordinary hedgerows, the class includes a windbreak type consisting of a low hedgerow and a line of trees, usually oaks (*Quercus* spp.), often more than 20 m apart.
(2) Hedges (H): barriers taller than hedgerows, forming a uniform vertical screen, mostly composed by a mixture of species, predominantly deciduous.

Table 2
Characteristics of windbreak classes of the study area

Class	n[a]	Length	Height		Width	
		Total (km)	Average (m)	C.V.[b] (%)	Average (m)	C.V.[b] (%)
Hedgerow	110	36.5	2.1	13.7	1.1	44.5
Hedge	64	18.4	8.8	26.6	4.8	68.8
Line 1	10	5.3	15.1	19.7	9.5	41.3
Line 2	13	3.9	12.5	23.6	6.2	45.2
Line 3	17	13.0	16.2	23.9	16.6	26.6
Wood	17	7.9	15.4	26.4	29.0	27.7

[a] n = number of observations.
[b] C.V. = coefficient of variation.

(3) Lines of coniferous trees (L1): a single or multiple lines of coniferous trees. Scots pine (*Pinus sylvetris* L.) is the most frequent species. This windbreak type presents medium-high porosity, with large gaps in the lower parts.
(4) Single lines of deciduous trees (L2): oaks (*Quercus* spp.) are dominant. Crowns are separated by large gaps. This type is usually located along field or road borders. Its main purpose is to provide shade; wind shelter is a secondary purpose.
(5) Multiple lines of trees, deciduous or mixed (L3): alleys or small woods of deciduous or mixed trees. Again, oak is dominant, but there is also much beech (*Fagus sylvatica* L.), lime (*Tilia cordata* Mill.), ash (*Fraxinus excelsior* L.), and maples (*Acer* spp). This type forms dense and tall barriers.
(6) Small woods (W): the ratio of barrier width/height is larger than 1. Species composition is usually mixed.

The attribution of windbreaks to a specific class was sometimes subjective. However, in the model, the classification affects only the porosity value, hence the classification of a windbreak that presented characteristics of more than one class was done on the basis of its apparent density.

Most of the network, more than 50% in length and number, is composed of hedgerows and hedges (Table 2). However, given their limited heights, these windbreaks provide little shelter. Tall lines of trees protect larger areas.

3.2. Porosity estimation

Optical porosity estimates are shown in Table 3. Generally, the porosity averages reflect field impressions: optical porosity is low for small woods, wide tree windbreaks, and hedgerows (classes W, L3, and He), medium for hedges (H), and high for coniferous and single line of trees (L1 and L2). Ranges and coefficients of variation reflect the in-class heterogeneity. In some cases, the mean squared deviation of the average estimation was larger than 10% due to the high variability within the class and the limited number of windbreaks belonging to it (classes L1 and L2). In the case of woods (W), optical porosity was lower than 0.20. Moreover, this type of windbreaks, together with multiple lines of trees (L3), are very wide (Table 2), and thus optical porosity is a poor estimator of aerodynamic porosity. In the WEPS model, the correction factor used in Eq. (8) to estimate

Table 3
Porosity estimations per windbreak class

Class	Porosity			
	Average	C.V.[a] (%)	Min	Max
Hedgerow	0.25	29.2	0.14	0.41
Hedge	0.32	32.8	0.16	0.55
Line 1	0.49	33.3	0.23	0.71
Line 2	0.46	27.7	0.14	0.73
Line 3	0.25	42.9	0.10	0.50
Wood	0.17	40.4	0.08	0.29

[a] C.V. = coefficient of variation.

barrier porosity from optical porosity and barrier width and height might therefore be inadequate. For dense barriers (classes L3 and W), better ways to estimate barrier porosity should be developed.

The optical porosity changes during the year, especially for deciduous species (Loeffler et al., 1992). The values in Table 3 reflect the average conditions of the summer period. For windbreaks rich in deciduous species like hedges (H), hedgerows (He), and single and multiple lines of trees (L2 and L3), the survey should be repeated in other periods to take into account the seasonal variability of optical porosity.

According to Kenney (1987), the recording distance does not affect the porosity accuracy. However, in our analysis it appeared that the longer the recording distance, the more important becomes the macroporosity. At large distances, the gaps in the crowns dominate the porosity estimation because the smaller pores between the leaves and branches tend to disappear from the image. Elements in the background were sometimes hard to separate from windbreak silhouettes, especially in the lower parts of pictures. This error was minimized by a careful choice of sample pictures or, when possible, by masking the background. The use of new image processing techniques, such as the intelligent "trainable" classification method proposed by Zhang et al. (1995), might give better results. The error in the porosity estimation caused by the choice of DN threshold value during the image-processing phase was small. A shift in the threshold value of plus or minus 25 DN over the original value resulted in changes in porosity of less than 2.5%. The image preprocessing might have introduced errors in porosity estimation, but the effects were considered negligible. Improvements can be introduced; however, Kenney's method proved to be a reproducible and quick field method to estimate windbreak porosity.

3.3. The GIS procedure

Fig. 4 shows the final friction velocity distribution for the experimental site during a westerly wind of 10 m s^{-1} at 10-m height. Windbreaks are shown as white lines. The gray tone represents the friction velocity value: the darker the gray tone, the lower the friction velocity. The friction velocity depends on both the land use, represented in homogeneous gray tones within the fields, and on the protection given by the windbreaks, visible as the shadow-like gray tones in the windbreak lees. The map shows the influence of the main windbreak characteristics on sheltering the surrounding areas. In point A of Fig. 4, for example, three windbreaks of increasing height shelter increasingly longer distances. Windbreak height has a large spatial effect on wind speed, as it determines the total sheltered area and the reduction factor at any distance from the barrier (Eq. (3)). Barrier porosity is also a major factor in the model predictions: it determines the friction velocity at any point in the windbreak lee, but its effect is reflected in the gray tone and is difficult to visualize. Windbreak width is important only in relation to height and porosity (Eq. (8)); its influence cannot be directly visualized in the image.

Point B of Fig. 4 shows the effect of the angle of incidence of wind vector and barrier orientation. Barriers that are increasingly parallel to the wind vector are less effective: the two windbreaks have similar height, but the total area sheltered by the southern barrier is much less than the shelter provided by the northern barrier. However, the model does not account for further reductions in sheltered area for winds oblique to barriers whose nature

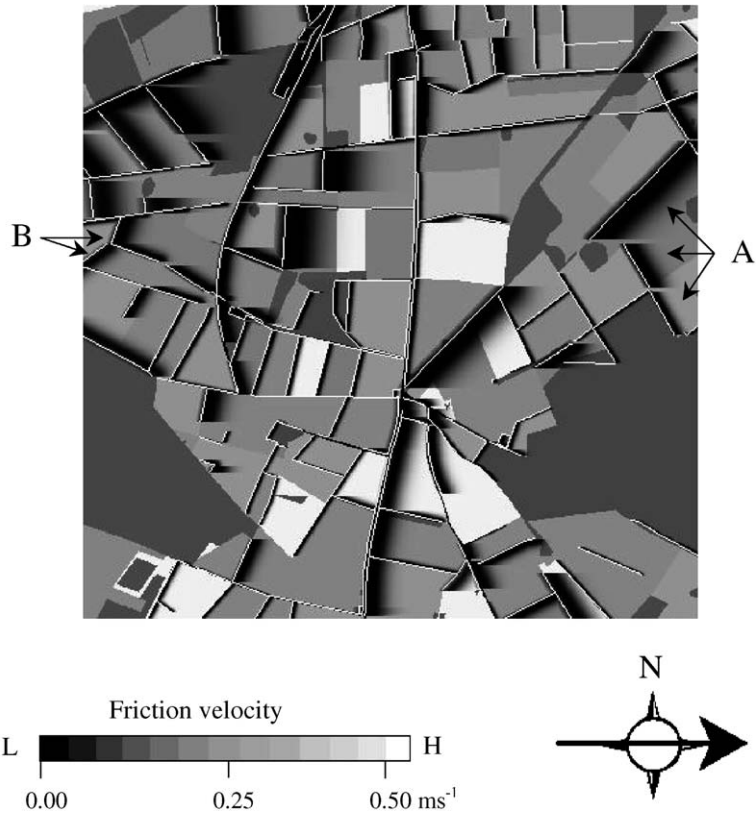

Fig. 4. The GIS model output for a western wind. Windbreaks are shown as white lines. Friction velocity is displayed in gray tones: the darker the gray tone, the lower the friction velocity. The arrow indicates the wind vector. Point A shows the influence of windbreak height on sheltered distances; point B shows the influence of the angle of incidence of wind vector with the windbreak. Map based upon Ordnance Survey Mapping with the permission of the controller of HMSO©Crown (Copyright Ed 2813360001).

is not geometrical. The relationship between reduction in shelter distance and barrier orientation–wind direction angle involves very complex interactions of turbulent wind flow and drag force caused by the windbreak (Wang and Takle, 1996). Numerical simulation models might give better insights in the future.

The second output of the model, i.e. the map that shows areas exposed to wind erosion risk, is not presented here. In order to make realistic predictions, the threshold value u_{*t} must be calculated according to soil conditions and land use types. At the moment, a procedure to calculate it is under development.

The application of the WEPS model, whose spatial scale is of a few adjacent fields at most, on a larger area introduces problems of upscaling. The windbreak routine, in particular, accounts only for the local shelter effects. Interactions between barriers are simplified by selecting the lowest reduction factor given by the barriers considered independently one from the other. This is not physically correct, but an appropriate

algorithm for the reduced effectiveness of successive barriers has not yet been defined. Again, numerical simulation models are likely to provide more insights in the future (Schwartz et al., 1997). Regional effects of windbreak networks may be even more important than local effects of single barriers, especially in the presence of an extensive windbreak system as in the study area, and could be included by measuring the landscape aerodynamic roughness height (Guyot and Seguin, 1978).

Notwithstanding these limits, the model permits an evaluation of wind speed reductions by windbreaks over large areas with a few basic parameters, thus allowing the integration of the windbreak protection in more extensive wind erosion prediction models. The model also permits the visualization of the influence of windbreak characteristics on the adjacent fields. Hence, it may become a valuable tool for windbreak design and scenario simulation purposes.

3.4. Windbreak network efficiency

Fig. 5 shows a comparison between wind vectors (r_j) and windbreak network shelter indices (SI_j). Vectors and indices are represented as fractions of their respective maximum along each direction, indicated in polar degrees with 0 set to north and clockwise progression. The graph shows that windbreak orientations were not optimal. The wind vector rose is highly asymmetrical: prevailing winds have WSW directions. The largest protection is oriented along the NNW–SSE axis (160–340°), while along the prevailing wind vector, shelter indices are at their minimum. However, the distribution of the shelter indices SI_j shows that windbreaks were not selectively oriented, but were mainly located

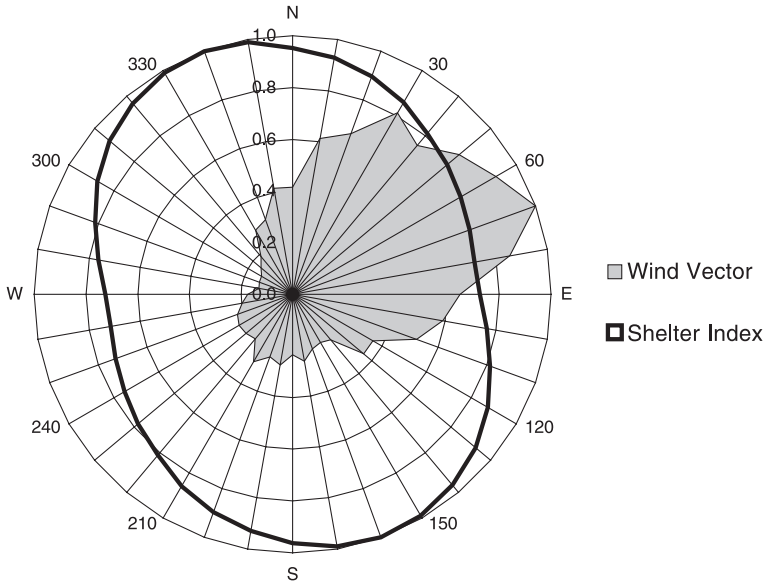

Fig. 5. Comparison between wind vectors (r_j) and windbreak network shelter indices (SI_j) for 36 directions. Vectors and indices are normalized by their respective maximum values.

along the field borders (Fig. 4). The network assures an almost homogeneous protection from all directions (Fig. 5): the range for directional shelter indices (SI_j) goes from 0.14 to 0.19, with an arithmetic average of 0.17 and coefficient of variation of 11.5%. The weighted mean shelter index for the area (SI, Eq. (11)) is low (0.16), meaning that the windbreak distribution is not optimal. The quantitative significance of the value of the synthetic shelter index SI, which was introduced with the present study, is difficult to evaluate for lack of terms of comparisons: insights in the future may be provided by running alternative scenarios on the same area. Further research on this topic is recommended.

The proposed shelter index SI limited the present study to an evaluation of wind speed reduction given by windbreaks. No consideration about the erosive power of wind and erodibility of soil was included. By limiting the analysis to erosive winds or to periods when soil is more exposed to erosion, the conclusions about the windbreak network effectiveness may be different. Unlike other indices proposed in literature (e.g. Zhang et al., 1995), the shelter index does not depend on critical friction velocity (u_{*t}), a parameter that depends on land use type. The shelter index SI was introduced to estimate the effectiveness of windbreak networks, extending the analysis of windbreak effectiveness to a larger landscape scale and accounting for the orientation of windbreaks in relation to different wind directions.

4. Conclusions

Spatial modeling of wind speed reductions by windbreaks requires some important problems to be solved. Notwithstanding their importance in crop protection, windbreaks are seldom treated explicitly in wind erosion models. The WEPS windbreak subroutine expresses the shelter effect as a function of distance from the barrier as well as windbreak height, porosity, width, and orientation.

The most difficult windbreak parameter to define is porosity. The optical porosity of digitized windbreak silhouettes (Kenney, 1987) is an imperfect estimator for analytical models of wind speed reduction, especially for wide barriers. It is important to develop an improved estimator, as windbreak porosity is the main input in the WEPS windbreak reduction factor. The use of color slides and a "trainable" image classification technique, as suggested by Zhang et al. (1995), may reduce the background interference and result in a better accuracy.

The GIS application of WEPS windbreak subroutine requires a limited number of input parameters. It models wind shelter considering both distance from the barrier and wind direction, two essential spatial aspects of the problem. It calculates the protection in terms of friction velocity reduction, so that it can be easily adapted to any physically based wind erosion model that applies the friction velocity as the driving variable for erosion. The theoretical limits of the model, i.e. the simplifications concerning the effects of multiple barriers and of oblique winds, and practical problems of its application, i.e. the use of optical porosity to estimate barrier porosity, should not be overlooked. However, the model shows the influence of windbreak characteristics on the protection at landscape level. Hence, it may become an interesting tool for windbreak design purposes.

The comparison between wind vector distribution and windbreak shelter index shows that the windbreak network provides good protection over the area, but the windbreak distribution is not optimal. However, focusing the analysis to more erosive winds or to periods when soil is at the highest erodibility conditions may lead to different conclusions about the windbreak network. The proposed shelter index SI can be considered a tool to estimate the effectiveness of windbreak networks at the landscape scale.

Further research should address the following: (1) the enhancement of the estimation of the aerodynamic porosity of living windbreaks; (2) the correction of predictions for wind directions oblique to the barrier; (3) the inclusion of the interactions between successive barriers; and (4) the inclusion of the regional effect of the windbreak network.

Acknowledgements

We thank the British Atmospheric Data Centre (BADC) for having granted access to the Met Office Land Surface Observation Stations Data and the British Ordnance Survey for permitting the use of the cartographic documents. We wish to thank also Mrs. and Mr. Headings and the Woodward family for their support and kindness during the fieldwork, and David Skidmore for his help with the GIS.

References

British Atmospheric Data Centre (BADC), 2000. Land Surface Observation Stations Data from the U.K. Met Office.

Cleugh, H.A., 1998. Effects of windbreaks on airflow, microclimates and crop yields. Agroforestry Systems 41, 55–84.

Drachenfels, O.V., 1994. Kartierschlussel fur biotoptypen in Niedersachsen, Stand Sept 1994. Naturschutz und Landschaftspflege in Niedersachsen A/4, 1–192.

ESRI, 1999. ArcInfo 7.2.1 Software and Reference Manual. ESRI, Redlands, USA.

Fryear, D.W., Saleh, A., Bilbro, J.D., Schomberg, M.M., 1998. Revised Wind Erosion Equation. Technical Bulletin No. 1. Agricultural Research Service, Lubbock, USA. USDA, 178 pp.

Guyot, G., Seguin, B., 1978. Influence du bocage sur le climate d'une petite region: resultats des mesures effectuees en Bretagne. Agricultural Meteorology 19, 411–430.

Hagen, L.J., 1991. A wind erosion prediction system to meet user needs. Journal of Soil and Water Conservation 46, 106–111.

Hagen, L.J., 1995. WEPS technical documentation: erosion submodel. WEPP/WEPS Symposium. Soil and Water Conservation Society, Ankeny, USA.

Heisler, G.M., Dewalle, D.R., 1988. Effects of windbreak structure on wind flow. Agriculture, Ecosystems and Environment 22–23, 41–69.

Kenney, W.A., 1987. A method for estimating windbreak porosity using digitized photographic silhouettes. Agricultural and Forest Meteorology 39, 91–94.

Loeffler, A.E., Gordon, A.M., Gillespie, T.J., 1992. Optical porosity and windspeed reduction by coniferous windbreaks in southern Ontario. Agroforestry Systems 17, 119–133.

McNaughton, K.G., 1988. Effects of windbreaks on turbulent transport and microclimate. Agriculture, Ecosystems and Environment 22–23, 17–39.

Nickling, W.G., 1994. Aeolian sediment transport and deposition. In: Pye, K. (Ed.), Sediment Transport and Depositional Processes. Blackwell, Oxford, UK, pp. 293–350.

Panofsky, H.A., Dutton, J.A., 1984. Atmospheric Turbulence. Wiley, New York, USA. 397 pp.

Riksen, M.J.P.M., De Graaff, J., 2001. On-site and off-site effects of wind erosion on European light soils. Land Degradation and Development 12, 1–11.

Schwartz, R.C., Fryrear, D.W., Juo, A.S.R., 1997. Simulation of wind forces and erosion in a field with windbreaks. Soil Science 162, 372–382.

Seguin, B., 1973. Rugosite du paysage et evapotranspiration potentielle a l'echelle regionale. Agricultural Meteorology 11, 79–98.

Wang, H., Takle, E.S., 1995. A numerical simulation of boundary-layer flows near shelterbelts. Boundary-Layer Meteorology 75, 141–173.

Wang, H., Takle, E.S., 1996. On the shelter efficiency of shelterbelts in oblique wind. Agricultural and Forest Meteorology 81, 95–117.

Wang, H., Takle, E.S., 1997. Momentum budget and shelter mechanism of boundary layer flow near a shelterbelt. Boundary-Layer Meteorology 82, 417–435.

Wilson, J.D., 1985. Numerical studies of flow through a windbreak. Journal of Wind Engineering and Industrial Aerodynamics 21, 119–154.

Zhang, H., Brandle, J.R., Meyer, G.E., Hodges, L., 1995. The relationship between open windspeed and wind speed reduction in shelter. Agroforestry Systems 32, 297–311.